

Francesco Cascone<sup>1</sup>, Pietro Roncioni<sup>1</sup>, Oreste Russo<sup>1</sup>, Marco Marini<sup>1</sup>, Sara Di Benedetto<sup>1</sup>, Marta Albano<sup>2</sup>, Roberto Bertacin<sup>2</sup>, Giuliano Ranuzzi<sup>2</sup>

CIRA, Italian Aerospace Research Centre, 81043 Capua, Italy
 ASI, Agenzia Spaziale Italiana 00133 Rome, Italy

#### **Abstract**

The present paper deals with the aerodynamic and propulsive characterization of a Hypersonic Scramjet System, i.e., a payload composed by Launch Vehicle (LV) and a flight demonstrator, the Scramjet Hypersonic Experimental Vehicle (SHEV), as part of a research project on experimentation for hypersonic flight and enabling technologies for future high-speed transportation systems, co-funded by CIRA and ASI. The winged rocket-based launch vehicle is conceived to bring at target altitude and velocity the SHEV, posing the challenge of designing and testing, at national level, a demonstrator capable of supporting a levelled hypersonic flight thanks to the introduction of a scramjet propulsion system.

Keywords: Scramjet, CFD, Hypersonic, Aerodynamic Database.

# 1. Introduction

The activities of the present paper are part of a research project aimed to develop, in the long term, a national hypersonic vehicle and related technologies by means of experimentation, in order to pave the way to future high-speed transportation systems. The project complements several initiatives born in Europe in the last 20 years: the various EU projects dedicated to hypersonic passenger flight (LAPCAT I&II, ATLLAS I&II, FAST20XX, HIKARI, HEXAFLY, HEXAFLY-INT, STRATOFLY) and the national initiatives that led to the design of prototypes such as, among others, the ZEHST French aircraft, developed by MBDA, ASTRIUM and ONERA, or the English SKYLON by Reaction Engines Ltd., which despite being more oriented towards supersonic flight and access to space, respectively, already included many of the technologies necessary for hypersonic flight. Hypersonic civil transport has always had as its weak point the low cruising autonomy, essentially linked to the too high fuel consumption. In recent years, a highly integrated design approach between efficient propulsion systems and high-lift configurations (LAPCAT-II and STRATOFLY configurations) is enabling the trend to be reversed ([1], [2], [3] and [4]).

The study on the Scramjet Hypersonic Experimental Vehicle (SHEV) starts from the experience gained thanks to the strong involvement of Italian companies, and CIRA in particular, in the European project HEXAFLY-INT (realization of a flight test of a glider without engine for hypersonic flight), and previously in the HEXAFLY one, posing the challenge of creating an aircraft capable of supporting a levelled hypersonic flight thanks to the introduction of a scramjet propulsion system ([5], [6] and [7]). The project is co-funded by the national research programme PRO.R.A. (Programma Nazionale di Ricerche Aerospaziali) and the Italian Space Agency (ASI), with the aim of designing a hypersonic propelled demonstrator capable of performing a levelled and controlled flight at Mach 6÷8 and an altitude of 28÷32 km, in order to realize and test in flight the enabling technologies for future civil transport systems at hypersonic speed.

This paper deals with activities that aim to verify the aerodynamic efficiency ( $L/D = 3 \div 4$ ) and the aero-propulsive balance (T>D) at Mach =  $6 \div 8$  in controlled flight of the demonstrator, and the aerodynamic database of the full system (i.e., the payload) composed by the launch vehicle and the above-mentioned demonstrator. In particular, the capability of the launch system to bring the demonstrator at the required altitude and velocity has to be verified in terms of stability,

maneuverability and trimmability. Another important point is the safe releasing of the SHEV vehicle by the launch system. For the purpose of verifying the above requirements numerical viscous CFD simulations were conducted for both the full system and the demonstrator in the experimental window in fuel-off and fuel-on conditions. For the SHEV, in particular, it is important to calculate the values of aerodynamic efficiency and air mass flow at the combustor inlet, and the verification of the aero-propulsive balance (T>D) that requires the development of reacting Hydrogen-Air simulations.

# 2. Mission and System Description

The preliminary mission concept envisages an air-launched solution with a carrier (stage I) capable of releasing the payload, composed by the propelled hypersonic demonstrator and the launch vehicle equipped with a booster, at a target point in terms of speed and altitude. From here the launch vehicle accelerates until it reaches the foreseen trajectory target point in terms of Mach and altitude, where the hypersonic propelled demonstrator is released and the scramjet must work for a time of at least 10 seconds.

It is therefore possible to identify three mission phases (Figure 1):

**Phase 0**: from the release of the payload from the carrier to the release of the demonstrator at the target point (Sep1 and Sep2 of Figure 1, respectively);

Phase 1: Experimental window (≥ 10 s);

Phase 2: Gliding phase.



Figure 1 - Mission Scenario

The launch vehicle connected to the propelled hypersonic demonstrator is represented in Figure 2.

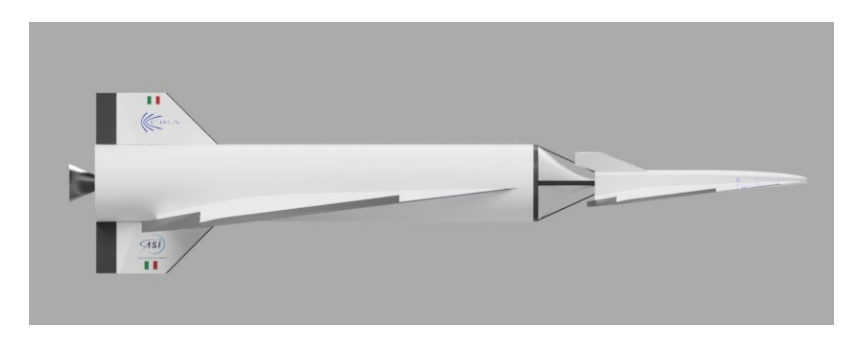


Figure 2 - Payload configuration.

The configuration of the propelled hypersonic demonstrator is based on the concept of "waverider", or a hypersonic vehicle with high aerodynamic efficiency in supersonic regime obtained through the exploitation of shock waves that form on the lifting surfaces, a phenomenon known as "compression lift". The demonstrator must also include a scramjet air-breathing propulsion system. The concept is depicted in Figure 3, and is a heritage of the already studied EU-FP7 HEXAFLY (see refs [5], [6], [7]).

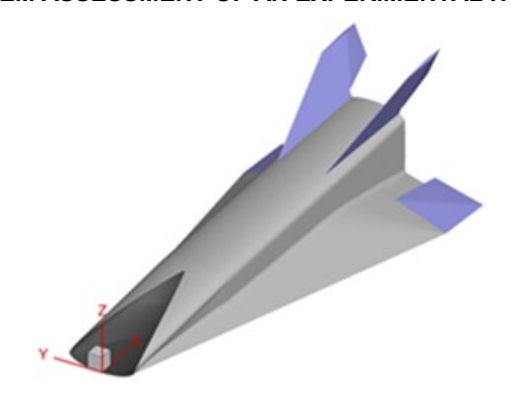


Figure 3 - Configuration of the SHEV vehicle.

# 3. Aerodynamic Database Building and Results

The AErodynamic Data Base (AEDB) building is the overall procedure that allows to obtain a full and integral set of information and/or data that characterize the aerodynamic environment in terms of flow field features, global and local forces and pressure distributions over the vehicle surfaces. In particular, the main parameters to be defined are:

- Components of aerodynamic forces and moments in function of the main variables characterizing the flight, i.e., Mach and Reynolds numbers, angle of attack, angle of sideslip, deflection of control surfaces, etc.
- Uncertainties levels to be added to the previous nominal data.
- Surface pressure distributions.

These data are inputs for several disciplines as flight mechanics, structural analysis, but also in some cases for propulsive database building.

The final and reliable aerodynamic database is foreseen to be obtained by means of both numerical and experimental activities.

This paper focuses on the preliminary study and aerodynamic characterization of the Payload (the scramjet hypersonic demonstrator coupled to the launch vehicle), which corresponds to the first phase of the mission (Figure 1).

The activities results are reported in terms of:

- Numerical aerodynamic database built by means of Inviscid CFD simulations for the Payload (LV + SHEV);
- Control surfaces effect;
- Trimmability and longitudinal stability based on AEDB preliminary results;
- Evaluations of some configuration improvements for the LV.

## 4. Aerodynamic Database

This section describes the operations performed in order to obtain the Aerodynamic Database (AEDB) for the Payload (Figure 2) which will be useful for conducting flight mechanics analyses ([8], [9], [10], [11], [12] and [13]). The aerodynamic database is provided as a function of Mach number ( $M_{\infty}$ ), angle of attack ( $\alpha$ ) and the elevon deflections ( $\delta_{\rm e}$ ). However, the analysis does not consider the effect of sideslip angle ( $\beta$ ). The reference quantities are reported in Table 1. The location of the Centre of Gravity is strongly variable due to the consumption of the burning solid grain of the booster.

Table 1 - Summary: Reference Quantities.

<i>y</i>	
Reference Length (L <sub>ref</sub> )	4.1248 m
Reference Surface (S <sub>ref</sub> )	4.7936 m <sup>2</sup>
Mass	17000 kg

# 4.1 Payload Clean Configuration

The calculation of the aerodynamic coefficients for the clean configuration of the Payload has been obtained by means of inviscid CFD simulations. The simulations have been carried out with using the commercial code ANSYS FLUENT®. Each solution is assumed to be convergent when the residuals drop more than three orders of magnitude, and the aerodynamic coefficients reach a constant value. The reference quantities (Table 1) considered for these calculations are the same already used for the SHEV, in order to obtain aerodynamic coefficients that are easily comparable with those already calculated for the demonstrator.

The full AEDB has been evaluated on two different meshes for subsonic and supersonic conditions in order to impose properly the far field conditions in all the directions.

The computational grids (*Figure 4*) have been generated using the ICEMCFD® software. The unstructured grids have about 7 million cells (for half configuration).

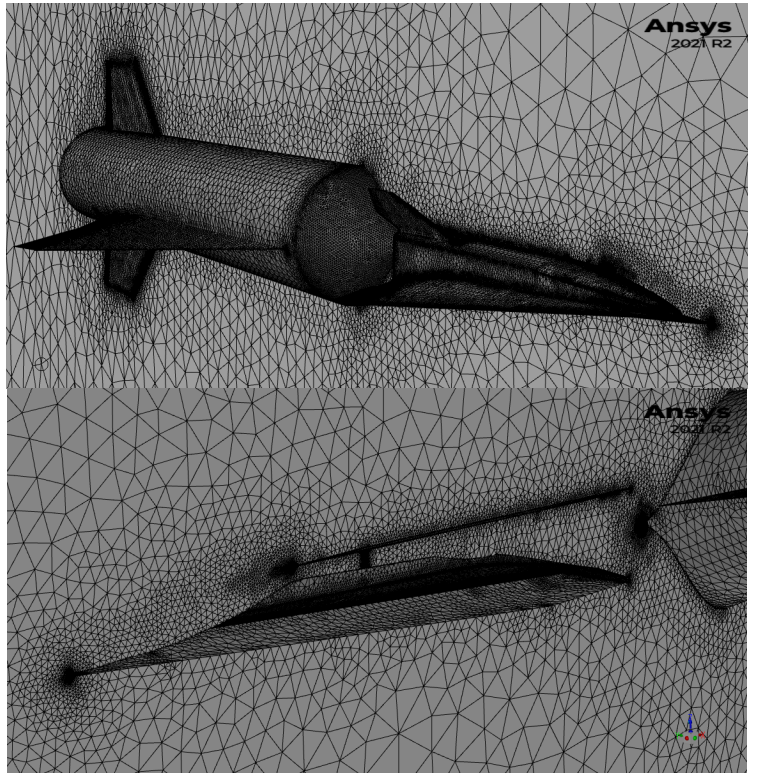


Figure 4 - Calculation grid for Payload inviscid simulations.

In addition, an adaptive mesh based on a density gradient criterion was employed in some regions (*Figure 5*), in order to capture the shock wave in the divergent nozzle of the SHEV when the asymptotic Mach number is not high enough ( $0.5 < M_{\odot} < 1.2$ ), and the curved shock that forms on the shaped cone of the Launch Vehicle.

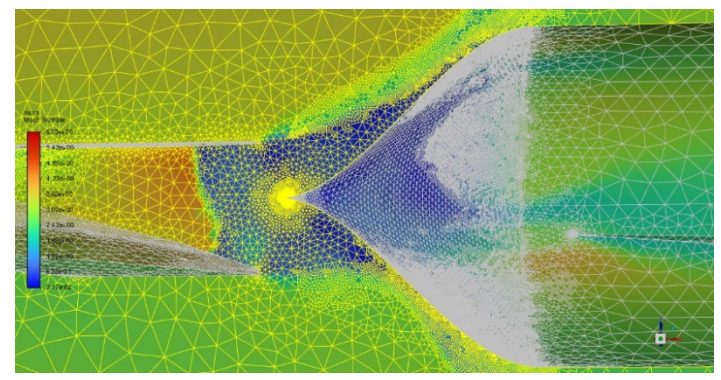


Figure 5 - Example of Adaptive mesh on FLS for M = 3.5.

The Payload aerodynamic coefficients as a function of Mach number and AoA are summarized in *Figure 6* and in *Figure 7*.

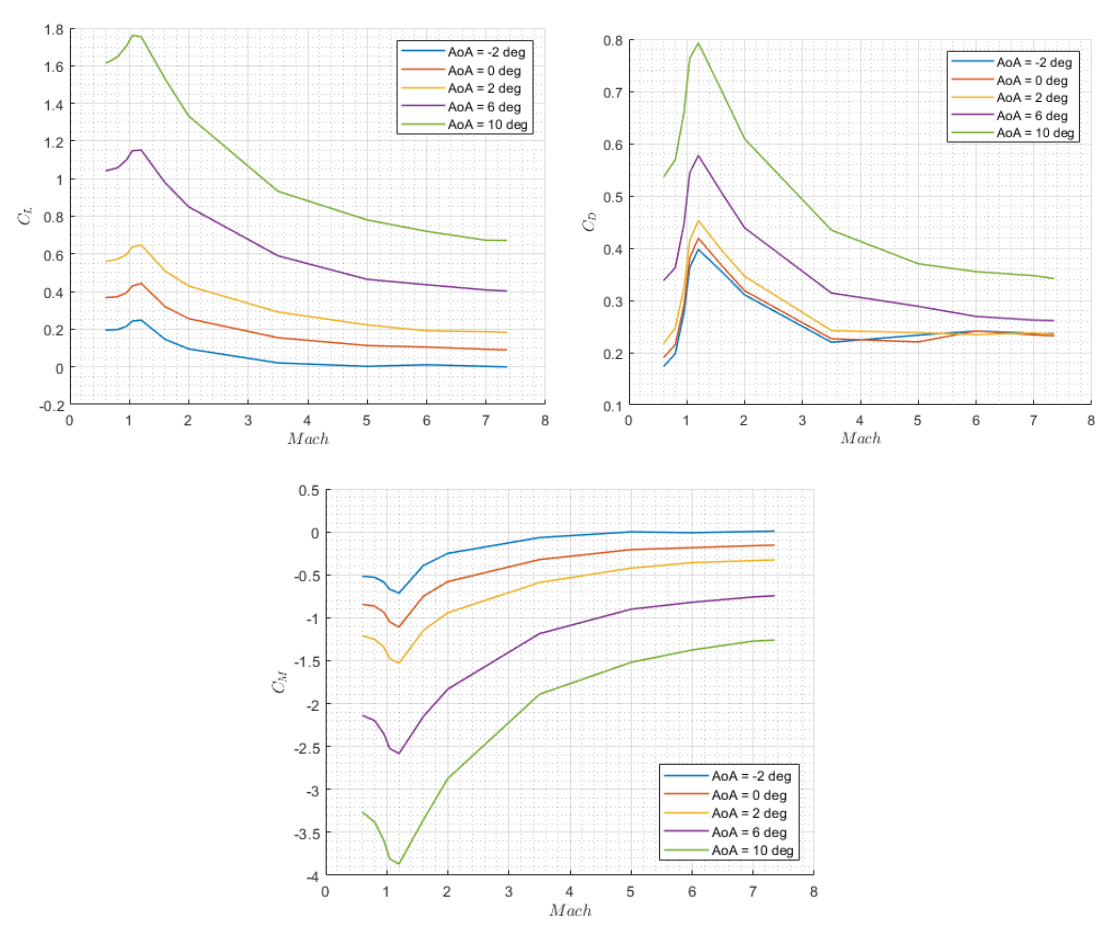


Figure 6 - Aerodynamic coefficients as a function of Mach number, varying AoA.

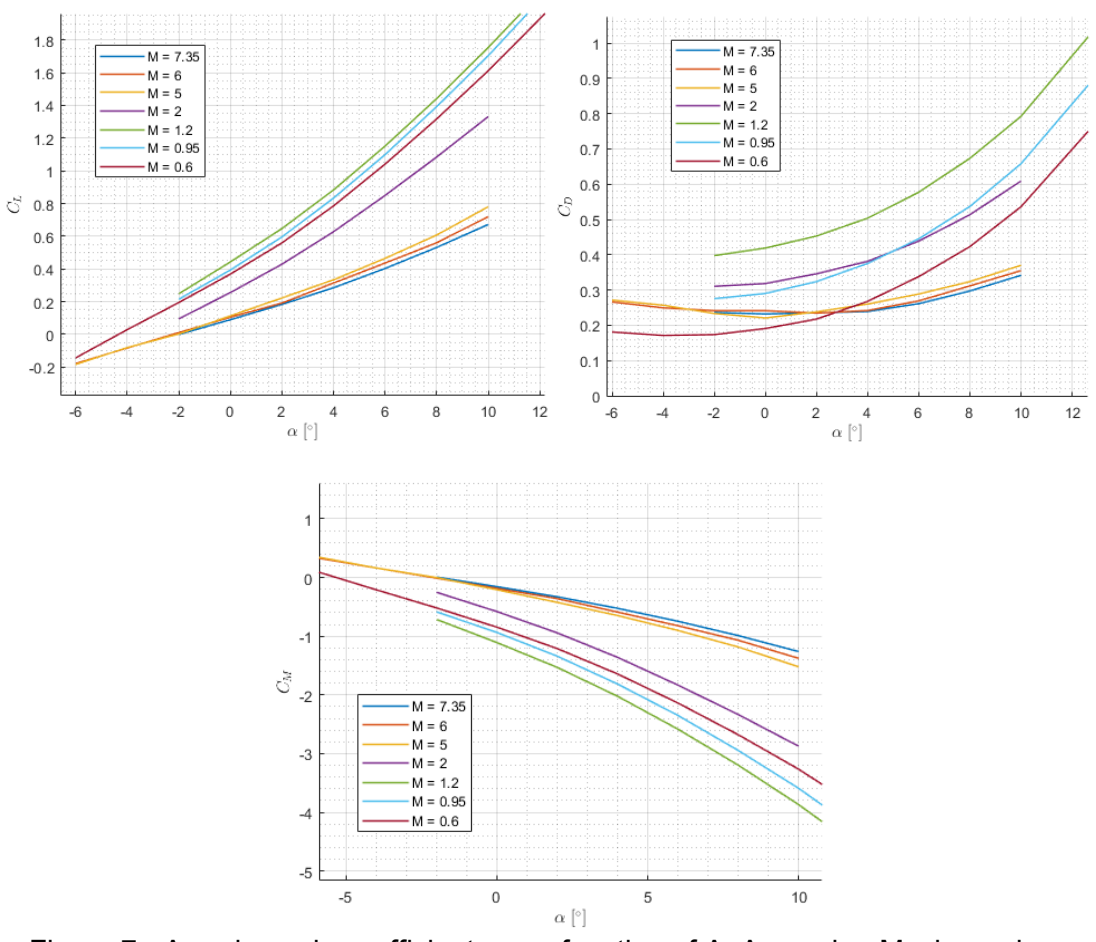


Figure 7 - Aerodynamic coefficients as a function of AoA, varying Mach number.

It is important to notice that the pitching moment coefficients displayed in *Figure 6* and in *Figure 7* are calculated with respect to the SHEV nose (X = Y = Z = 0 m). The coefficients reported in these figures are representative of the AEDB and characterize the aerodynamics of the LV taking into account the approximations made. Despite the complexity of the system, no particularly relevant characteristics emerge, except for transonic conditions where the coefficients undergo strong variations (as expected). For what concerns the LV, the CoG is varying over time due to the burning of the solid propellant, therefore it is not possible to evaluate its longitudinal stability without an in-depth mission analysis. Despite this, for illustrative purposes, *Figure 8* shows the  $C_M$  relative the CoG position estimated at the moment of ignition of the solid propellant (x = 8.875 m behind the SHEV nose).

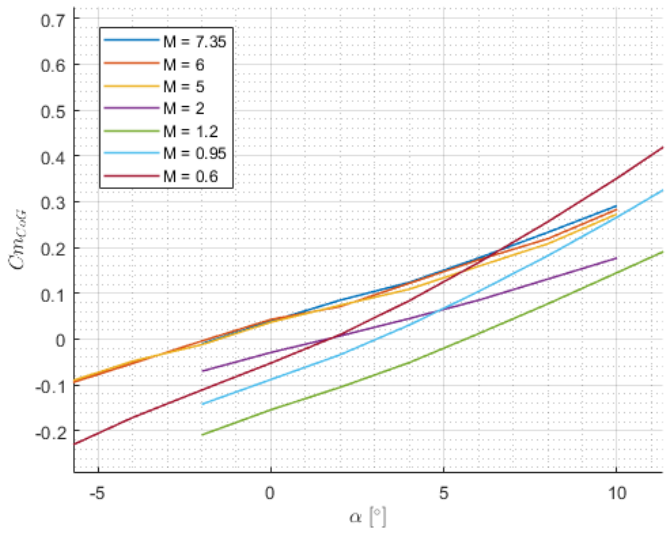


Figure 8 - Pitching moment coefficient relative to CoG, as a function of AoA, varying Mach number.

As shown in Figure 8, the unstable nature of the Payload configuration clearly emerges due to the positive derivative of the pitching moment coefficient computed with respect to the *CoG*. However, it must be taken into consideration that the slope of these curves will vary over time due to the shifting of the *CoG*.

Then, assuming a linear variation of the Mach number with increasing altitude, it was possible to apply a viscous correction [10] to the drag coefficient (*Figure 9*). In this way it is possible to take into account the increase in drag due to viscosity.

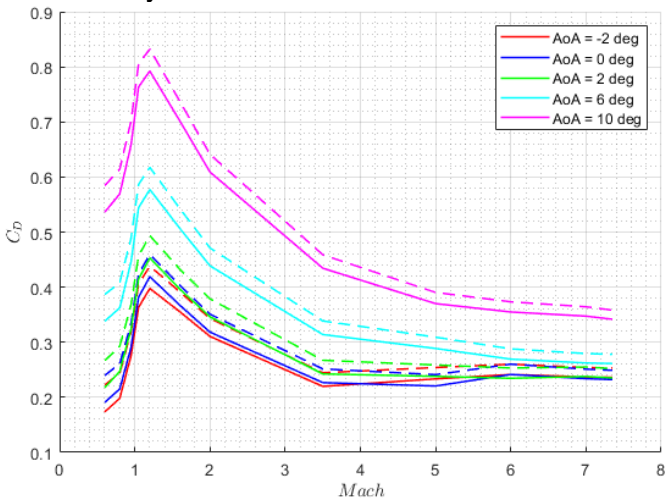


Figure 9 - Comparison between inviscid drag coefficient (solid lines) and viscous drag coefficient (dashed line) as a function of Mach number.

From the CFD simulations carried out, it was observed that the presence of the LV behind the SHEV during the launch ascent trajectory causes a shock wave inside the nozzle of the SHEV itself. This effect is felt up to  $M_{\infty}=5$ ; once this Mach number is exceeded, the increase in pressure caused by the shaped cone is unable to rise back inside the nozzle, which is then able to eject out the normal shock in the nozzle.

The impact of the presence of LV is showed in *Figure 10* for  $M_{\infty} = 3.5$ .

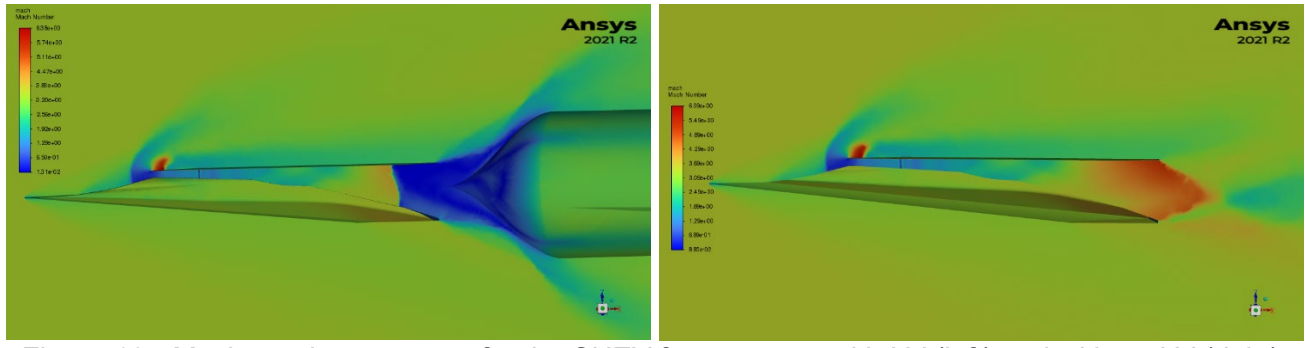


Figure 10 - Mach number contours for the SHEV for  $M_{\infty} = 3.5$  with LV (left) and without LV (right).

This effect can also be described by comparing the lumped aerodynamic coefficients of the SHEV, when the LV is present and when it is not present (see *Figure 11*). As expected, exceeding  $M_{\infty} = 5$ , they coincide: SHEV can't be influenced by the presence of LV because the flow field is supersonic, therefore the pressure disturbances caused by LV itself cannot propagate upstream.

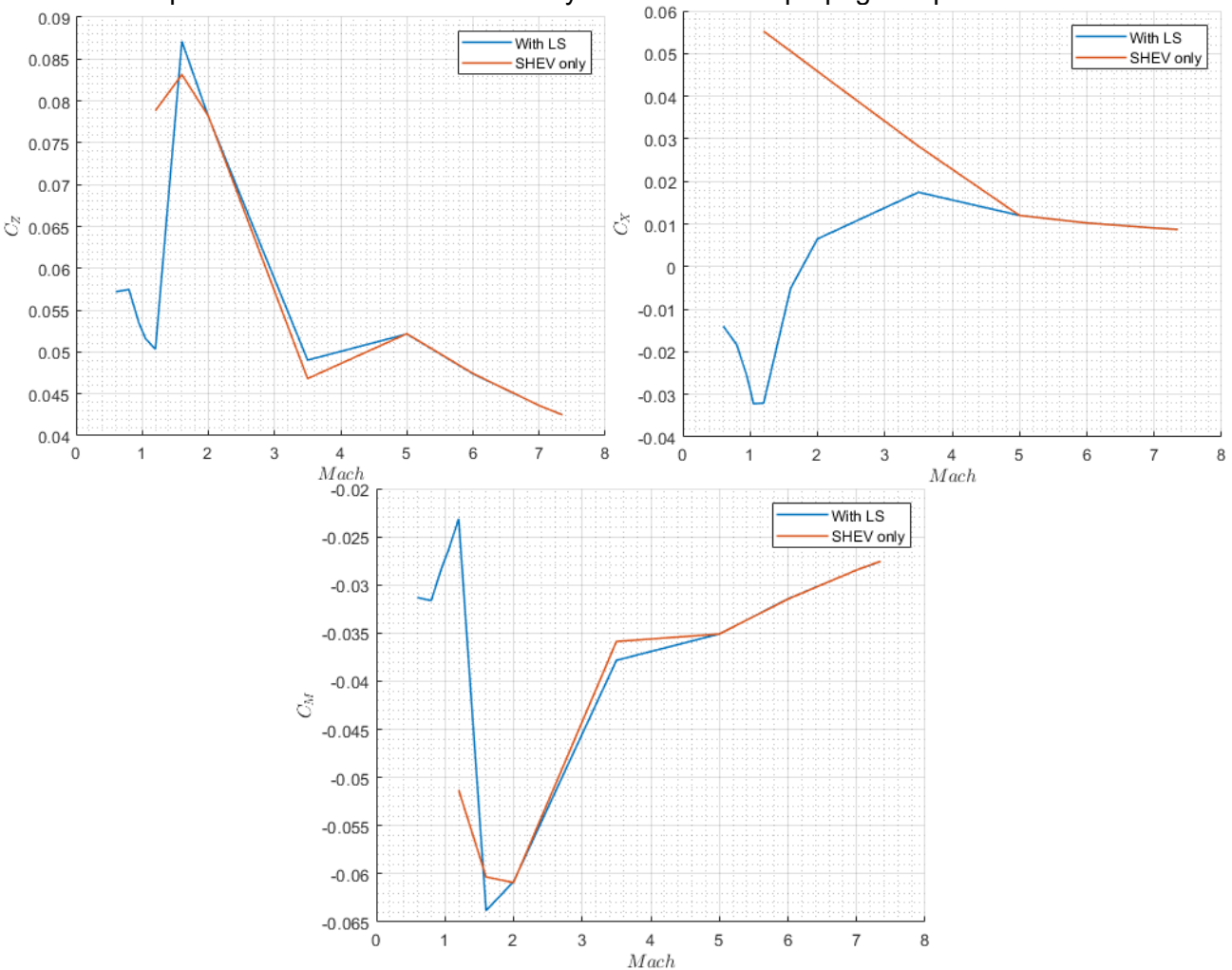


Figure 11 - SHEV aerodynamic coefficients, with LV (blue line) and without LV (red line).

It is also interesting to note that for low Mach numbers, the increase in pressure on the LV cone induces a negative drag coefficient (therefore thrusting) on the SHEV.

## 4.2 Control Surfaces Effect

This section describes the aerodynamic analysis in terms of the variation of aerodynamic coefficients evaluated along the wind axis, i.e., the lift coefficient ( $C_L$ ), drag coefficient ( $C_D$ ), and pitching moment coefficient ( $C_M$ ) versus the control surface deflection (i.e. the elevons). The impact of elevon's deflection on aerodynamic coefficients has been evaluated for SHEV, and then scaled for LV, as it will be seen below. The SHEV aerodatabase with deflected control surfaces is reported hereinafter.

The variation of the aerodynamic coefficients is assessed as the difference between the aerodynamic coefficients of the configuration evaluated with deflected elevon and the coefficients evaluated with the undeflected elevon, i.e., considering the pitching moment coefficient as:

$$\Delta C_{M}(\delta_{e}) = C_{M_{\delta_{e}}} - C_{M_{\delta_{e}=0}}$$
 (1)

In order to calculate data for elevon's effect, a simplified configuration constituted by the wing and the elevon has been considered (*Figure 12*), and CFD simulations have been performed with the inviscid flow hypothesis.

The following ranges have been analyzed to generate the longitudinal aerodynamic data sets:

- $0.6 \le M_{\infty} \le 7.35$
- $-6^{\circ} \le \alpha \le 10^{\circ}$
- $-20^{\circ} \le \delta_e \le 10^{\circ}$

As an example, the Pitching Moment Coefficient of the flapped wing is reported in *Figure 13* for some Mach numbers, varying the AoA and the elevon deflection.



Figure 12 - Grid for a stand-alone wing with a deflected elevon.

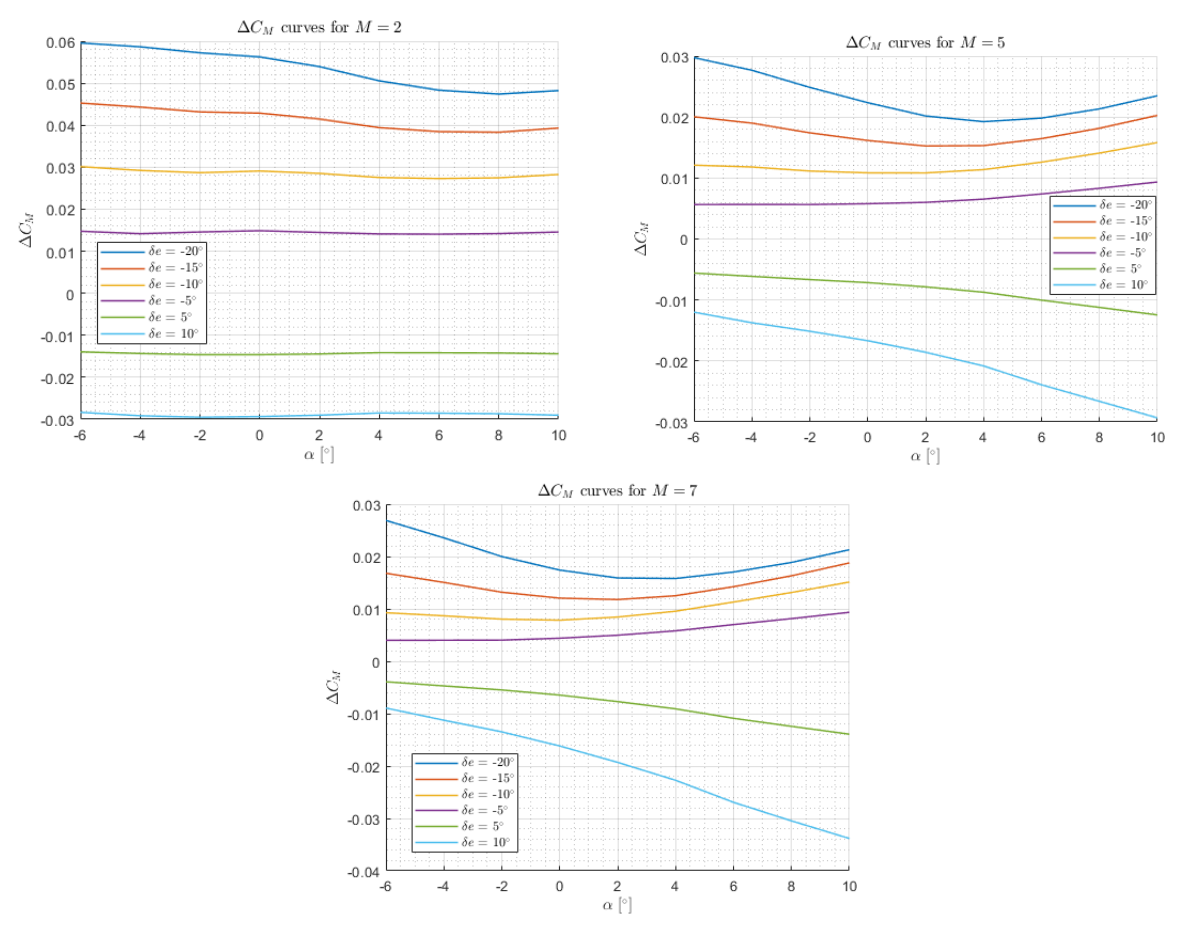


Figure 13 - Effect of Flap Deflection on Pitching Moment Coefficient for different Mach numbers.

The wing of the LV (with its elevon) is an upscaled version of the SHEV's wing, thus allowing us to assume that the effect of the elevon of the LV is the same of the SHEV's elevon (previously calculated), of course properly upscaled. In reality, this is not accurately valid due to energy loss through the curved shock on the shaped cone, but this hypothesis is reasonably acceptable in the current stage of the project.

The aerodynamic coefficients of the forces ( $\Delta C_L$  and  $\Delta C_D$ ), have been simply scaled by means of elevons wet surface ratio (this ratio is about 3.95):

$$\Delta C_{L_{LV}} = \Delta C_{L_{SHEV}} \cdot \frac{S_{LV}}{S_{SHEV}} \tag{2}$$

$$\Delta C_{D_{LV}} = \Delta C_{D_{SHEV}} \cdot \frac{S_{LV}}{S_{SHEV}} \tag{3}$$

Instead, the pitching moment coefficient has been scaled by means of the same surfaces' ratio, and also the ratio between the respective distances from the SHEV nose:

$$\Delta C_{M_{LV}} = \Delta C_{M_{SHEV}} \cdot \frac{S_{LV}}{S_{SHEV}} \cdot \frac{d_{LV}}{d_{SHEV}}$$
(4)

The distances "d" should be evaluated from the SHEV nose to each elevon's pressure center: for simplicity purpose, the geometric center of elevons has been considered (the ratio of distances is about 3).

For illustrative purposes, the results for M = 7.35, 1.05 and 0.6 are reported in *Figure 14* and *Figure 15* (note that the pitching moments are computed with respect to the SHEV nose). The effect of the deflection of the elevon in both directions (+10 deg, -20 deg) is reported in *Figure 16* for M = 7.35 varying the AoA. Finally, the impact of the deflection of the elevon in both directions is also reported for AoA =  $6^{\circ}$  varying the Mach number in *Figure 17*.

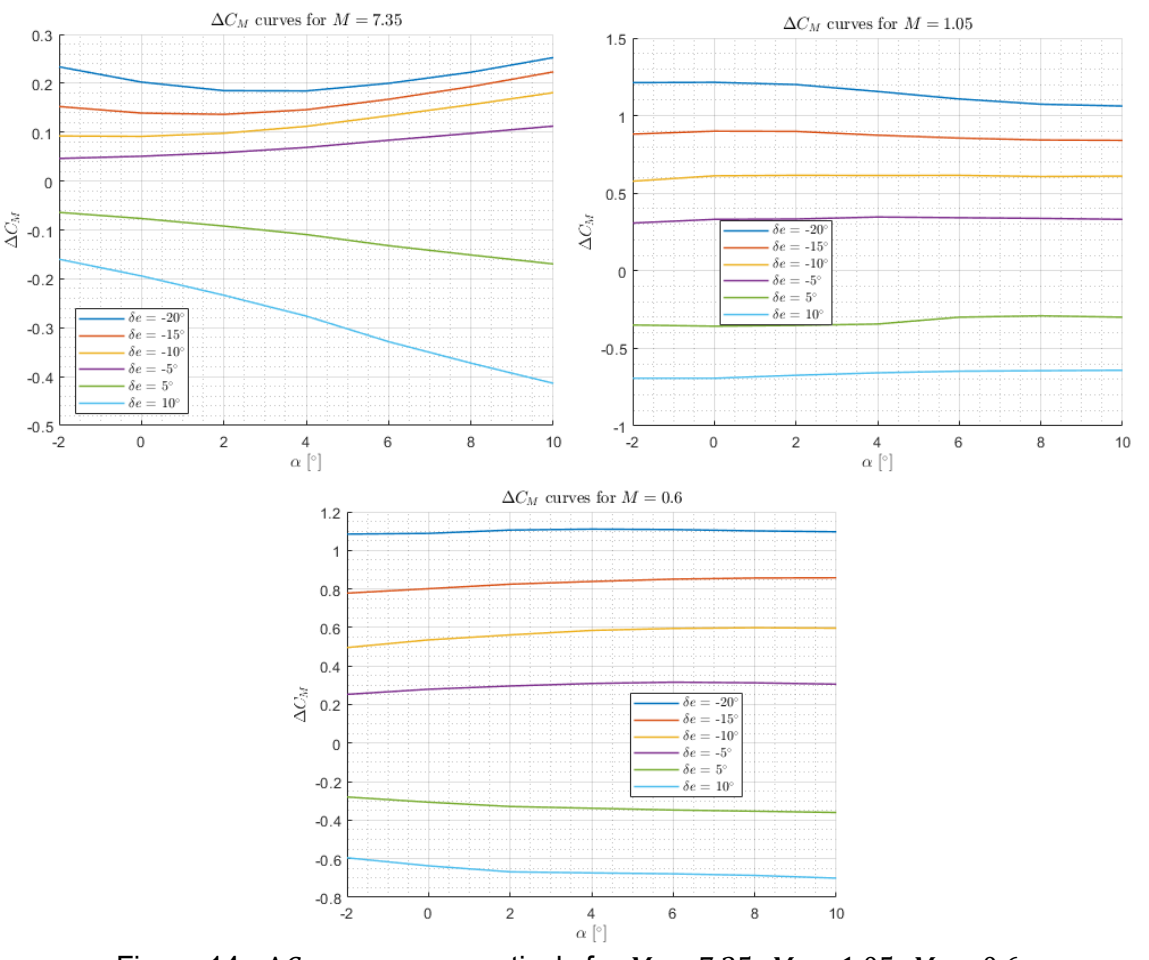


Figure 14 -  $\Delta C_M$  curves respectively for M = 7.35, M = 1.05, M = 0.6.

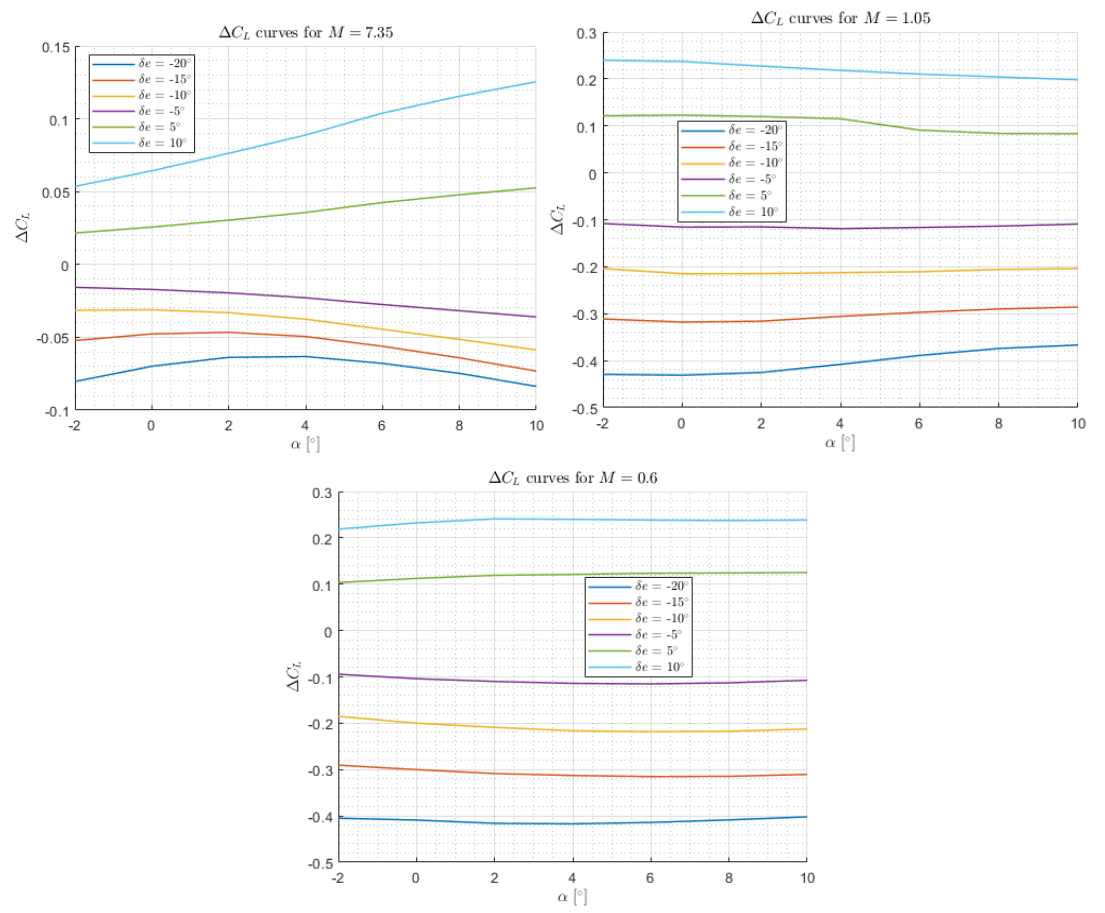


Figure 15 -  $\Delta C_L$  curves respectively for M = 7.35, M = 1.05, M = 0.6.

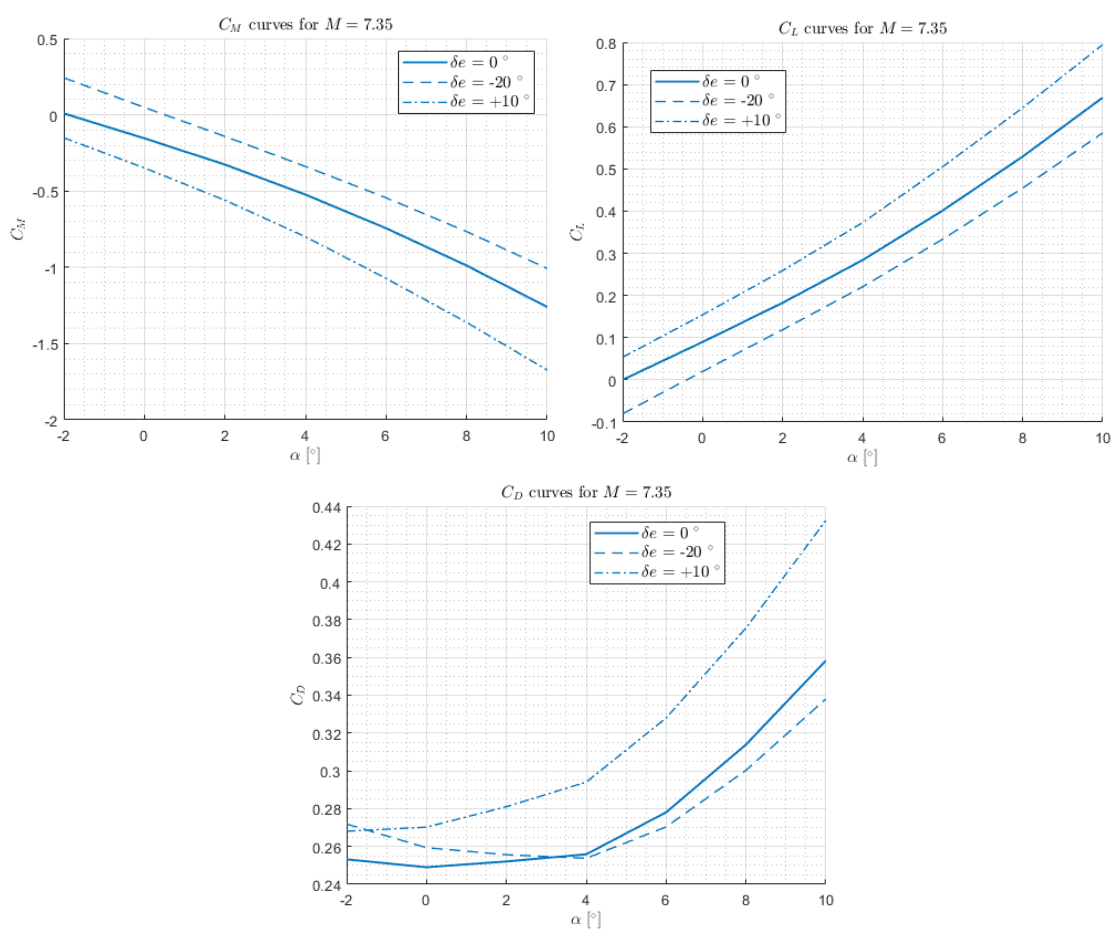


Figure 16 – Effect of elevon deflection on aerodynamic coefficients for M = 7.35.

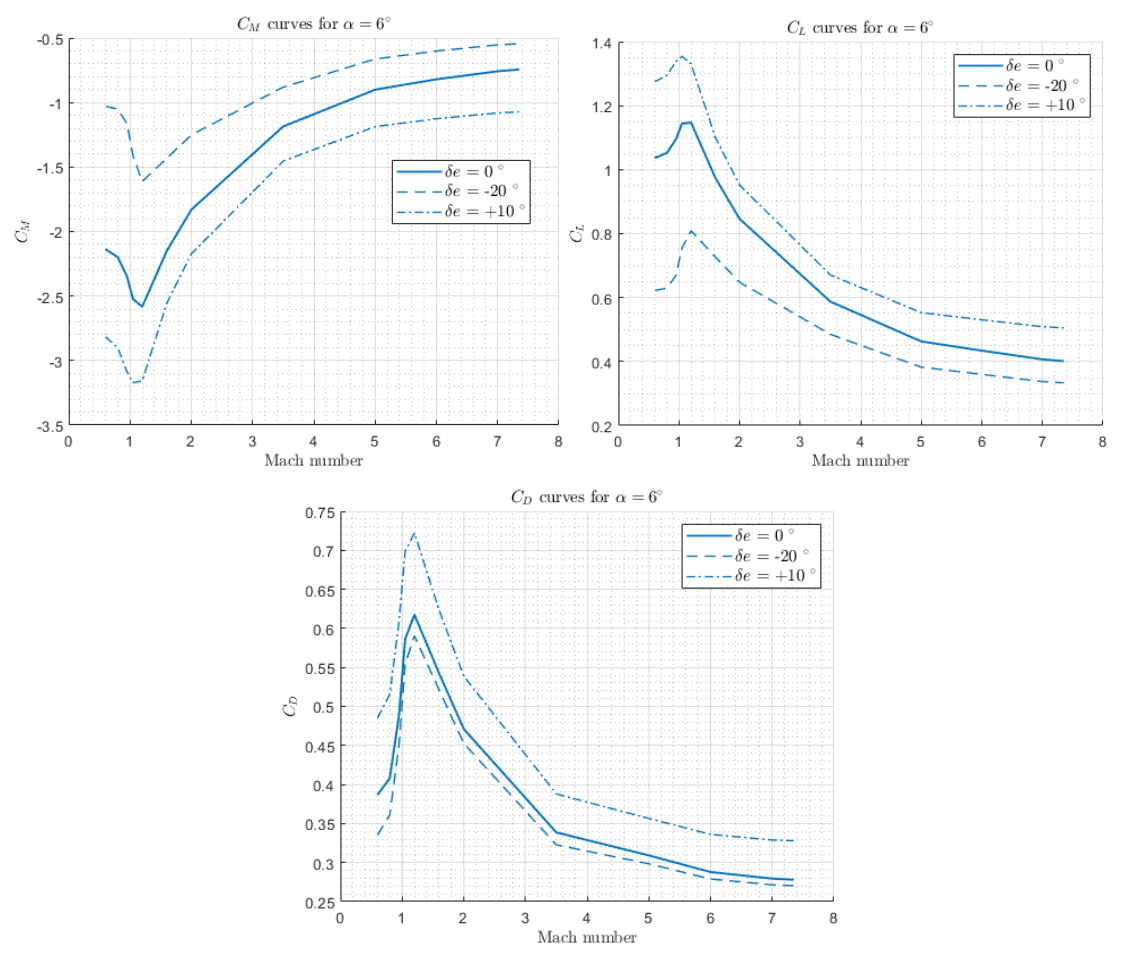


Figure 17 - Effect of elevon deflection on aerodynamic coefficients for AoA = 6°.

# 5. Trimmability and Stability

Starting from the AEDB, it is possible to verify the trimmability and stability of the Payload configuration under certain assumptions.

Assuming the thrust trend of the Orion 50 ST ([14] and [15]) and considering also the possible use of the rocket with thrust vectoring (TV) control ( $\pm 5^{\circ}$ ), a constant flight path angle (FPA = 12°), and the variation of the mass over the time (varying due to the burning of solid propellant, as shown in *Figure 18*), it is therefore possible to perform a preliminary check on flyability of the Payload.

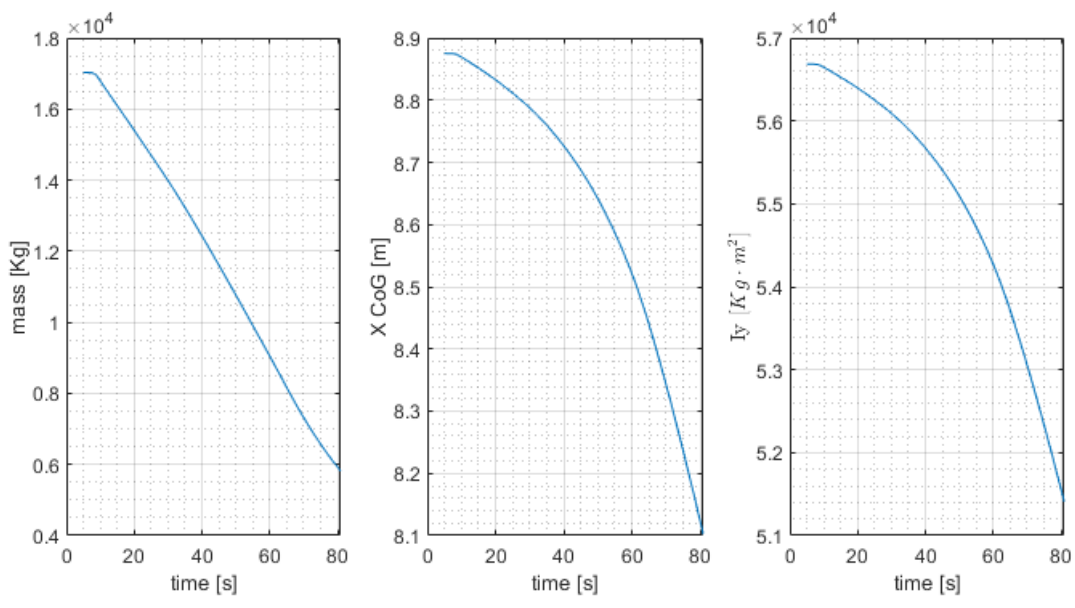


Figure 18 - Mass, CoG and longitudinal inertia variation over the time for Payload.

## 5.1 Trimmability

Starting from the release of the payload from the carrier (M ≈ 0.6, altitude ≈ 13 Km, Sep1 in Figure 1), knowing the aerodynamic characteristics of the payload as a function of M, AoA and δe, and considering the assumptions done in the previous section, it is possible to make a preliminary check of the Payload trimmability. It is possible to do that for each Mach number, finding the couples of AoA and  $\delta_e$  that trim the Payload (root of the following system of equations):

$$\begin{cases} mV\frac{d\gamma}{dt} = T \cdot \sin(\alpha + \varepsilon_T) + L(M, \alpha, \delta_e) - W \cdot \cos\gamma \\ M_A(M, \alpha, \delta_e) + M_T = 0 \end{cases}$$
 (5)

The two equations of the system are coupled, and their solution allow us to get the AoA and elevon for known conditions. Then, it is possible to update the Mach number and the altitude by solving the following equations:

$$m\frac{dV}{dt} = T \cdot \cos(\alpha + \varepsilon_T) - D(M, \alpha, \delta_e) - W \cdot \sin\gamma$$

$$\frac{dh}{dt} = V \cdot \sin\gamma$$
(6)

$$\frac{dh}{dt} = V \cdot \sin \gamma \tag{7}$$

Eq. 7 represents the update of altitude over the time, useful to calculate the dynamic pressure (International Standard Atmosphere model has been assumed). The thrust vectoring angle has been assumed variable in order to guarantee a trimming condition for each Mach number.

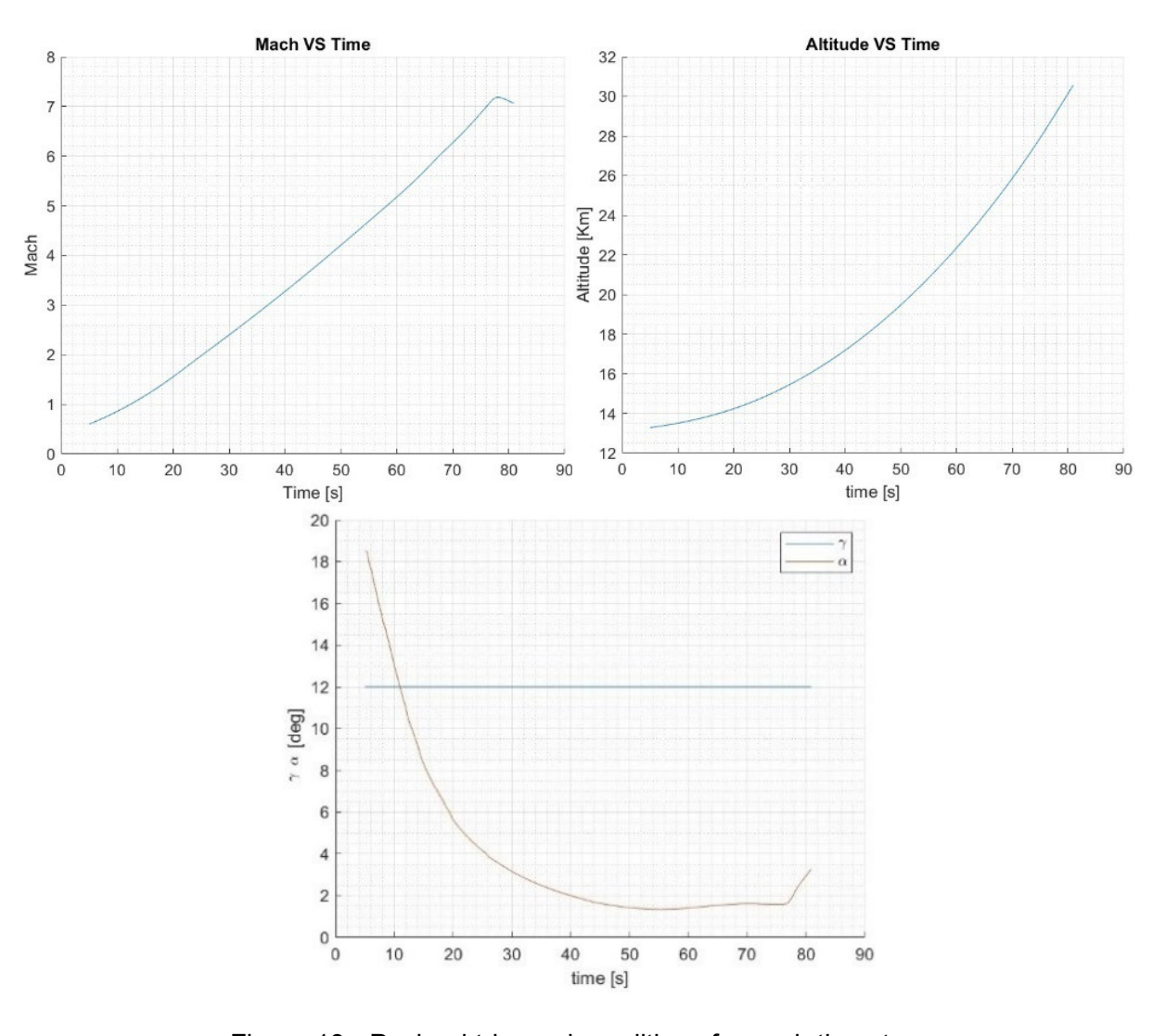


Figure 19 - Payload trimmed conditions for each timestep.

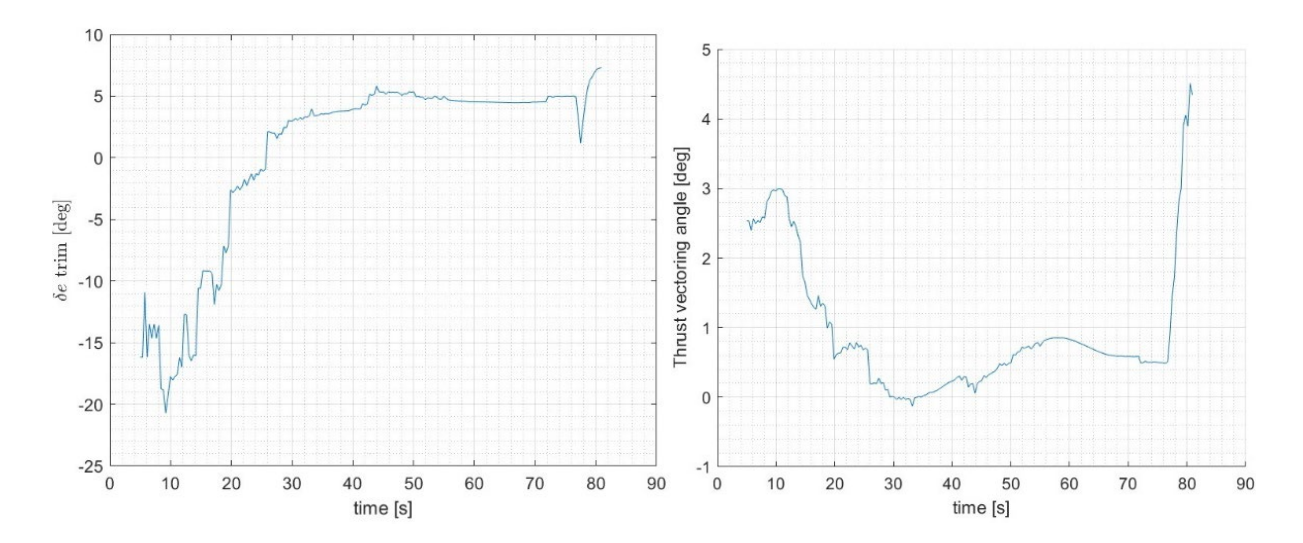


Figure 20 – Elevon deflection and Thrust vectoring to guarantee payload trimmed conditions for each timestep.

The preliminary results shown in *Figure 19* and *Figure 20* allow us make some considerations:

- 1. With the assumptions made, the altitude and Mach number for the demonstrator test can be reached;
- 2. For low Mach number, a very high AoA should be considered to obtain a trimmed condition, due to the dynamic pressure still too low;
- 3. For each flight condition, an AoA exists that trims the Payload (however, it depends on  $\gamma(t)$  and  $\varepsilon_T(t)$ );
- 4. The final altitude is depending on  $\gamma(t)$ . The shown trajectory brings to an altitude greater than 30 Km. However, modifying  $\gamma(t)$  does not impact significantly the final Mach number;
- 5. It must be considered that a constant  $\gamma(t)$  has been used in previous equations. A non-constant  $\gamma(t)$  will cause a centrifugal force, changing the AoA of trim. For example, a pull-down manoeuvre (  $\frac{d\gamma(t)}{dt} < 0$  ) causes a centrifugal force that adds to the lift: for the trim, a minor AoA would be necessary.

## 5.2 Longitudinal Stability

Now, it is possible to verify the stability condition for the LV. In order to have a stable vehicle, the centre of gravity must stay ahead of the centre of pressure (Cp). The centre of pressure can be defined as:

$$X_{cp} = -\frac{C_m}{C_z} \cdot L_{ref} \tag{8}$$

where  $C_m$  is the pitching moment coefficient with respect to the nose of the SHEV. This is reasonably true when  $C_z \neq 0$ . The coefficients are relative to the clean configuration ( $\delta_e = 0^{\circ}$ ).

From Figure 21 it seems clear that the Payload is not longitudinally stable, with the considered assumptions. This can be explained by considering that the presence of the SHEV ahead of the Launch System contributes greatly to the forward positioning of the center of pressure. It immediately becomes clear that it is not possible to move the CoG forward as too much ballast would have to be added and the structure would become too heavy.

Another way, that of moving the Payload centre of pressure backwards, seems to be more feasible, although it involves some changes of the geometry: a possibility is to shift back the wing, otherwise is possible to substitute the upper Vertical tail with two V-Tails.

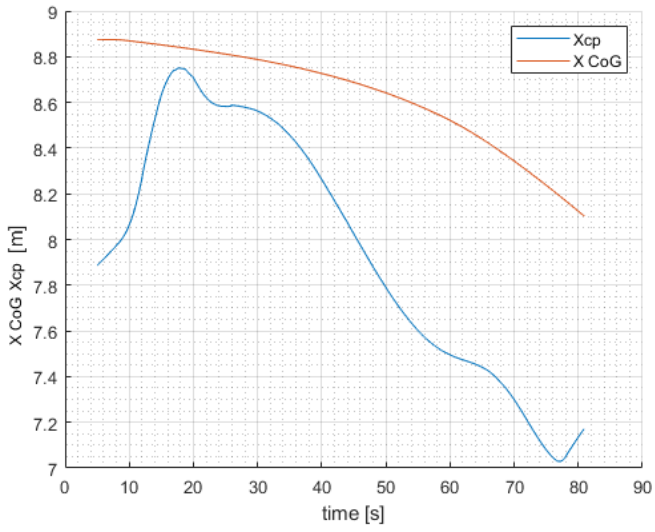


Figure 21 - Comparison between CoG and Cp.

## 5.2.1 Configuration Changes to improve Longitudinal Stability

A trade off was made between three different configurations:

- 1. Wing shifted backwards up to the LV base (about 1.4 m);
- 2. Upper Vertical tail substituted by two V-Tails (rotated by 60° with respect to the symmetry plane);
- 3. Both modifications.

For illustrative purposes, only the third configuration is reported in *Figure 22*.

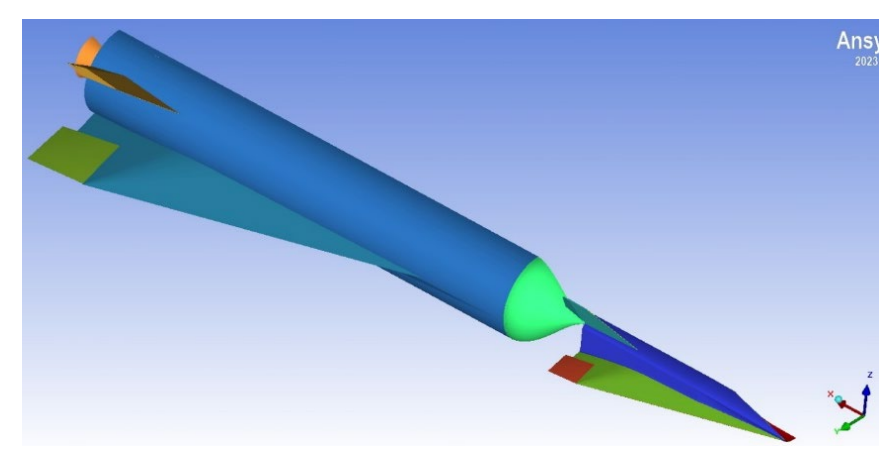


Figure 22 - LV+SHEV configuration with shifted wing and V-tails added.

The effects of these geometry modifications are preliminarily and simply evaluated by the principle of superposition.

To get an idea of how stabilizing is the backwards shifted wing, it was assumed that the lift and drag coefficients of the insulated wing are the same, but that only the moment coefficient had changed due to the shift along X axis of the wing's pressure centre.

The new pitching moment coefficient has been evaluated as following:

$$C_{M_{wing}} = C_{M_{wing}} \cdot \frac{X_{cp_{wing}} + \Delta s}{X_{cp_{wing}}}$$
(9)

where  $\Delta s$  is wing's translation (about 1.4 m has been considered).

An AEDB for the isolated V-Tail only has been computed, as a function of Mach and AoA. For subsonic and transonic conditions, CFD simulations were carried out. For supersonic conditions, the shock-expansion method has been implemented to evaluate the aerodynamic coefficients,

considering the different entropy levels due to the upstream curved shock.

Then, the aerodynamic coefficients have been simply summed to the ones of the old AEDB.

In order to get a longitudinally stable LV for each Mach number, both of these improvements were necessary. By simply modifying the AEDB with the method just mentioned, new trimmability conditions were found and the conditions for stability for each Mach number were reassessed. Figure 23 shows that with these hypotheses, the pressure center is positioned behind the center of gravity, thus obtaining a longitudinally stable configuration.

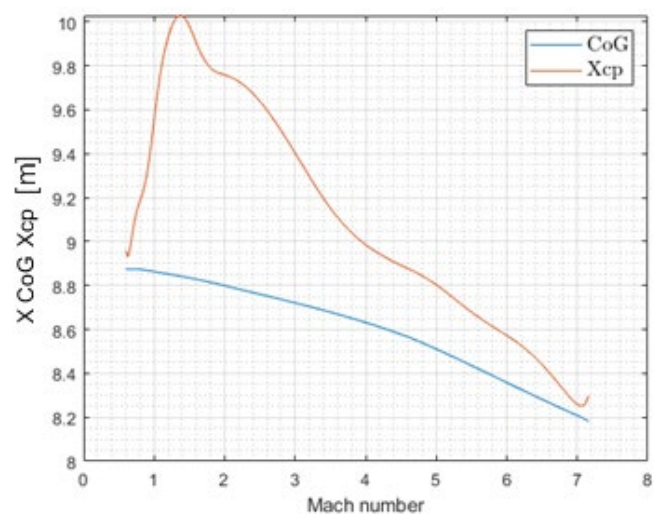


Figure 23 - Comparison between pressure center and center of gravity for the new configuration.

Figure 24 shows for some Mach numbers that the Pressure Centre is always located behind the Centre of Gravity, also varying the AoA:

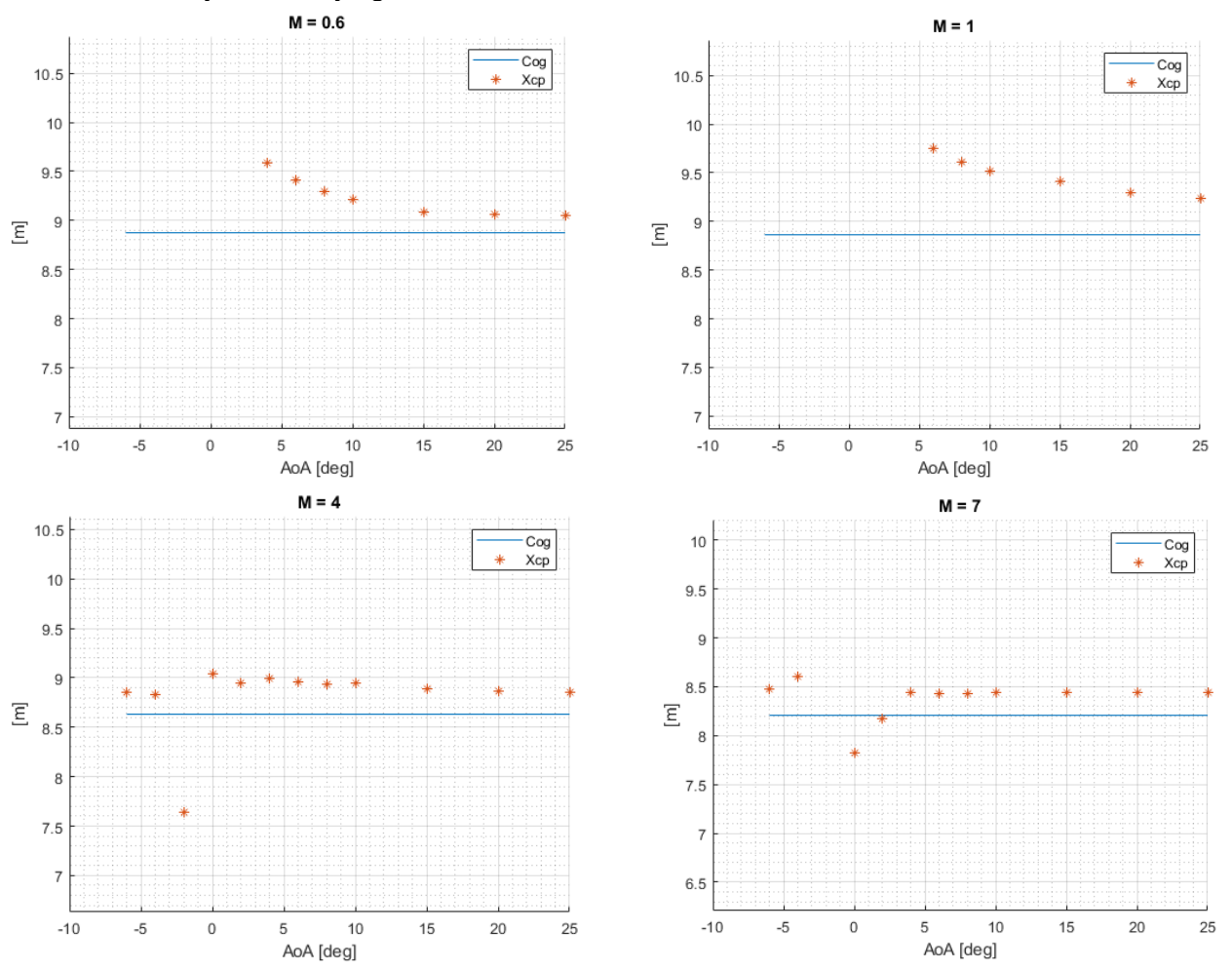


Figure 24 - Xcp and CoG positions VS AoA for some different Mach number.

However, it should be noticed that this analysis is given by a simple superposition principle, and it was therefore not possible to take into account the effects of the downwash, or the finiteness of the wing for the V-tail in supersonic conditions (the coefficients were calculated with shock-expansion method). In order to prove the actual improvement of this new configuration, new CFD calculations were performed for two specific AoAs (one high and one low). The calculations were also made on the configuration with the vertical tail (configuration 1), to quantify the improvement due to the addition of a tail.

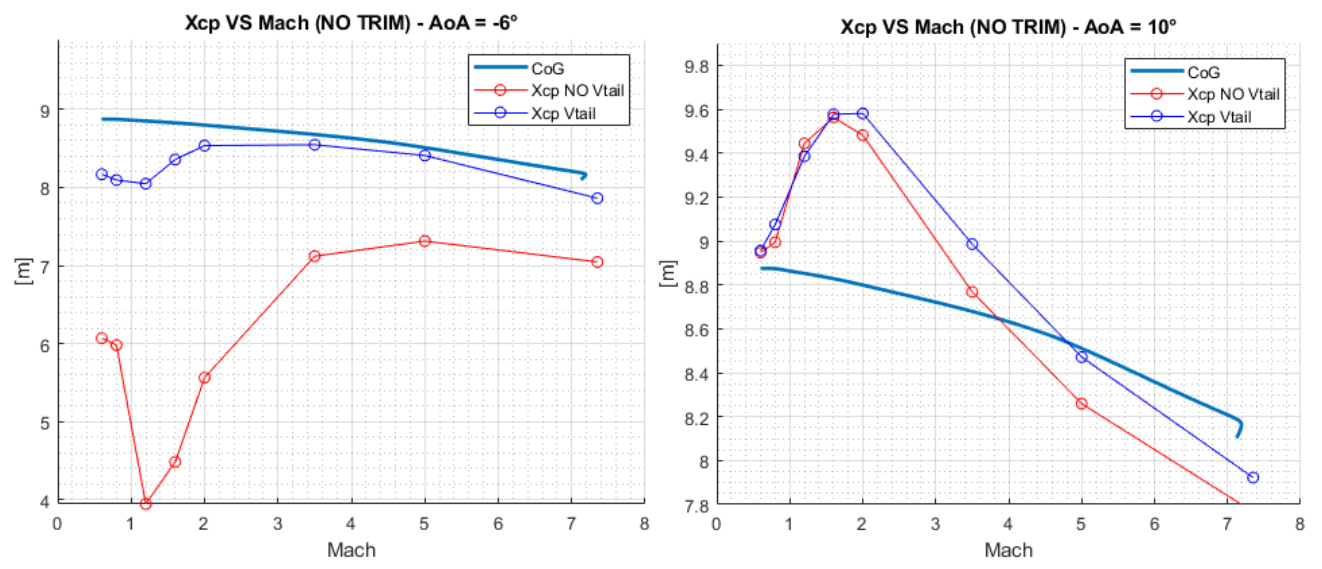


Figure 25 - Pressure Center VS Center of Gravity for AoA = -6° (left) and AoA = 10° (right).

As shown previously in *Figure 20*, in the first half of trajectory we expect to have a high AoA, while in the second half a low AoA is expected. Furthermore, a pull-up maneuver is expected in the first half  $\frac{d\gamma(t)}{dt} > 0$  causing the necessity of a higher AoA for trim. Vice versa for the second half of the trajectory: we expect therefore a lower AoA (even a negative one).

This observation is useful for analysing the results in *Figure 25*. In fact, for a low AoA (left figure) the pressure center is almost near the center of gravity for high Mach number. Instead, for low Mach number must be considered the right figure: it shows a large static stability margin.

The presence of V-Tail is necessary for the second part of trajectory, when you have an high Mach number and low AoA (left figure).

The improvements brought by the configuration with shifted wing and V-Tail, seem to allow a longitudinal stability for almost all the trajectory hypothesized, increasing the reliability of the mission. A new full AEDB will be generated by CFD calculations, in order to allow a deeper flight mechanics analysis.

#### 6. Conclusions

This paper reports the first results of the AEDB characterization for the Launch Vehicle obtained mainly from inviscid CFD simulations (*Figure 6* and *Figure 7*) and a viscous correction (*Figure 9*). Then, a preliminary study on longitudinal stability and trimmability has been reported.

The main results can be summarized as follows:

- The payload (SHEV + LV) has been characterized from the aerodynamic point of view;
- The effect of elevon has been evaluated by means of inviscid CFD calculations, producing an AEDB, useful for conducting a preliminary flyability analysis (*Figure 14* and *Figure 15*);
- The trajectory analysis has shown the ability to perform the mission for what concerns trimmability all over the range of Mach. This configuration can't allow longitudinal stability (Figure 19 and Figure 20);
- New configurations have been evaluated by means of simplified methods, in order to guarantee a longitudinally stable behavior, shifting the wing behind and adding two V-Tail upward (Figure 22);

• The AEDB of the Payload (new configurations with and without V-Tails) has been evaluated by CFD in some points of interest, in order to prove the improvements (*Figure 25*).

For the full payload, future activities will involve a check on lateral-directional stability. Additionally, a dedicated interface system between SHEV and LV will be studied, which has not been considered so far. After these activities, a new AEDB will be produced for the entire payload.

Although it has not been elaborated in this paper, activities on the SHEV are also underway in parallel. In particular, a study is being conducted to assess the impact of the equivalence ratio on thrust.

## 7. Contact Author Email Address

mailto: f.cascone@cira.it

# 8. Copyright Statement

The authors confirm that they, and/or their company or organization, hold copyright on all of the original material included in this paper. The authors also confirm that they have obtained permission, from the copyright holder of any third party material included in this paper, to publish it as part of their paper. The authors confirm that they give permission, or have obtained permission from the copyright holder of this paper, for the publication and distribution of this paper as part of the ICAS proceedings or as individual off-prints from the proceedings.

# **Acknowledgements**

The work has been co-funded by Italian Space Agency and CIRA ScPA in the frame of the agreement nr. 2022-13-HH.0-F43D22000410005.

## References

- [1] J. Steelant, R. Varvill, C. Walton, S. Defoort, K. Hannemann, M. Marini, "Achievements Obtained for Sustained Hypersonic Flight within the LAPCAT-II Project", AIAA-2015-3677, 20th AIAA International Space Planes and Hypersonic Systems and Technologies Conference, July 06-09, 2015.
- [2] E. Blanvillain, G. Gallic, "HIKARI: Paving the way towards High Speed Air Transport", *AIAA-2015-3676*, 20th AIAA International Space Planes and Hypersonic Systems and Technologies Conference, July 6-9, 2015.
- [3] Mack A., Steelant J., Adirim H., Lentsch A., Marini M., Pilz N., "FAST20XX: Achievements on European Suborbital Space Flight", *7th European Symposium on Aerothermodynamics*, Brugge, Belgium, May 2011.
- [4] J. Steelant et al., "Achievements obtained within ATLLAS-II on Aero-Thermal Loaded Material Investigations for High-Speed Vehicles", 21st AIAA International Space Planes and Hypersonics Technologies Conference, 6-9 March 2017, China.
- [5] J. Steelant et al., "Conceptual Design of the High-Speed Propelled Experimental Flight Test Vehicle HEXAFLY", AIAA-2015-3539, 20th AIAA International Space Planes and Hypersonic Systems and Technologies Conference, Glasgow, Scotland, U.K., July 6-9, 2015.
- [6] G. Pezzella, M. Marini, M. Cicala, A. Vitale, T. Langener, J. Steelant, "Aerodynamic Characterization of HEXAFLY Scramjet Propelled Hypersonic Vehicle", *AIAA-2014-2844*, *AIAA Aviation*, *32nd AIAA Applied Aerodynamics Conference*, 16-20 June 2014, Atlanta, GA, USA.
- [7] Di Benedetto S., Di Donato M.P., Schettino A., Scigliano R., Nebula F., Morani G., Cristillo D., Marini M., Cardone S., Steelant J., Villace V., "The high-speed experimental flight test vehicle of HEXAFLY-INT: a multidisciplinary design", CEAS Space Journal, published online on 5 January 2021, DOI: 10.1007/s12567-020-00341-5.
- [8] Viola N., Fusaro R., Saracoglu B., Schram C., Grewe V., Martinez J., Marini M., Hernandez S., Lammers K., Vincent A., Hauglustaine D., Liebhardt B., Linke F., Fureby C., "Main Challenges and Goals of the H2020 STRATOFLY Project", *Aerotecnica Missili & Spazio* (2021) 100:95–110, Published online: 29 May 2021, https://doi.org/10.1007/s42496-021-00082-6.
- [9] Roncioni P., Vitagliano P. L., De Gregorio F., Pezzella G., Romano L., Paglia F., "Aerodynamic Appraisal of the VEGA-C Launcher", *JSR-Journal of Spacecraft and Rockets*, 24 April 2023, http://arc.aiaa.org | DOI: 10.2514/1.A35610.

- [10]Viola N., Roncioni P., Gori O., Fusaro R., "Aerodynamic Characterization of Hypersonic Transportation Systems and Its Impact on Mission Analysis", *MDPI-Energies*, 16 June 2021, https://doi.org/10.3390/en14123580.
- [11]S. Defoort, L. Serre, R. Grenon, Narmada, "ZEHST: Environmental challenges for hypersonic passenger transport", AIAA 2012-5873, 18th AIAA/3AF International Space Planes and Hypersonic Systems and Technologies Conference, September 2012.
- [12]U. Mehta, M. Aftosmis, J. Bowles, S. Pandya, "SKYLON Aerodynamics and SABRE Plumes", AIAA 2015-3605, 20th AIAA International Space Planes and Hypersonic Systems and Technologies Conference, Glasgow, Scotland, U.K., July 6-9, 2015.
- [13]Bahm C., Baumann E., Martin J., Bose D., Beck R.E., Strovers B., "The X-43A Hyper-X Mach 7 Flight 2 Guidance, Navigation, and Control Overview and Flight Test Results", *AIAA/CIRA 13th International Space Planes and Hypersonic Systems and Technologies*, May 2005, Capua, Italy. AIAA-2005-3275.
- [14]Di Benedetto S., Marini M., Roncioni P., Vitale A., Vernillo P., Di Lorenzo G., Scigliano R., Cardone S., Albano M., Bertacin R., "The Scramjet Hypersonic Experimental Vehicle", HiSST-2024, *The 3rd International Conference on High-Speed Vehicle Science Technology*, 14 -19 April 2024, Busan, Korea.
- [15]Northrop Grumman. Orion Motor Series Catalogue. <a href="https://cdn.prd.ngc.agencyq.site/-/media/wp-content/uploads/Orion-Motor-Series.pdf">https://cdn.prd.ngc.agencyq.site/-/media/wp-content/uploads/Orion-Motor-Series.pdf</a>